InAs/GaAs core–shell nanowires

ARTICLE *in* CRYSTAL GROWTH & DESIGN · AUGUST 2011

Impact Factor: 4.89 · DOI: 10.1021/cg200393y

CRYSTAL GROWTH & DESIGN

ARTICLE

pubs.acs.org/crystal

InAs/GaAs Core−Shell Nanowires

Ronit Popovitz-Biro,[‡] Andrey Kretinin,[†] Palle Von Huth,[‡] and Hadas Shtrikman*[,†]

[†]Braun Center for Submicron Research, [‡]Microscopy Unit, Weizmann Institute of Science, Rehovot, Israel 76100

ABSTRACT: Gold-assisted vapor−liquid−solid (VLS) growth of InAs nanowires was optimized and used for growth of highly mismatched InAs/GaAs core−shell heterostructure nanowires having the wurtzite structure. The motivation is 2-fold, providing means for surface passivation of InAs nanowires (NWs) for electronic devices and ballistic transport applications on one hand and for studying the structural properties of a highly mismatched system in a core−shell, cylindrical configuration on the other hand. The misfit between the InAs core and the mostly relaxed GaAs shell was deduced from the average spacing between the edge dislocations, the periodicity of the Moiré fringes resulting from the overlap between the InAs and GaAs lattices and the splitting in the electron diffraction images. Both line and loop edge dislocations are formed in the strain relaxation process. The experimental radial and axial misfits were found to be approximately 6 ± 1% and 4 ± 0.5%, respectively.

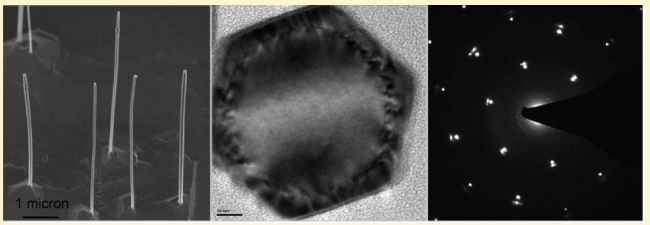

INTRODUCTION

The growing interest in InAs nanowires (NWs) as promising objects for one-dimensional quantum transport experiments is stimulated by their reduced dimensionality, large g-factor,[1,2] strong spin−orbit interaction,[3] and existence of the surface accumulation layer. The particular interest in InAs NWs is motivated by the fact that the combination of their properties makes them suitable for hosting the theoretically predicted and still undetected Majorana bound states.[4,5] As long as the transport in InAs NWs takes place in close vicinity to the surface, the problem of controlling the quality of the NW surface becomes one of the main objectives for the growth process optimization. The most efficient method of reducing the influence of the surface states is passivation of the semiconductor NWs surface with a shell having a different composition, first applied to the Si/Ge system in a cylindrical core−shell NW configuration by Lauhon et al.[6] Wider band gap InP was later successfully applied as a shell to passivate InAs NWs and improve their device performance.[7−9] Theoretical work by Yann-Michel Niquet[10,11] looks into the electronic properties of InAs NWs embedded in a GaAs shell, which has been applied by Paladugu et al. who studied the formation of both axial and radial InAs-GaAs heterostructures[12−15] and by Kavanagh and co-workers.[16] The work described in this paper extends from the growth of bare InAs NWs on the (111)B crystallographic plane of InAs, to the growth of core−shell InAs/GaAs NWs with a wurtzite structure, utilizing the control of low NWs density to ensure suitable conditions for growth of a uniform shell with no shadowing effects. The highly uniform morphology of the core−shell NWs achieved provides a perfect system for the study of strain relaxation in a cylindrical configuration.

EXPERIMENTAL SECTION

InAs NWs and core−shell InAs/GaAs NWs were grown in a Riber molecular beam epitaxy (MBE) system using the Au-assisted vapor−liquid−solid (VLS) method. InAs NWs were grown on (111)B InAs after in situ evaporation of a thin gold layer and a short heating under arsenic overpressure to form the gold catalyst droplets. Growth of the GaAs shell was done under similar growth conditions as for the core, for a period ranging between 10 and 60 min (the growth details are given in a previous review[17]). Post growth cool down of the core−shell samples was done by ramping down the temperature at a rate of 10 °C/min. We adjusted the growth conditions to obtain uniform coating all along the NW and minimized the bending at the top of the NW. To obtain uniform coating along the NW, the growth temperature of the shell was lowered to 390 °C so as to eliminate the accumulation of material toward the tip of the wire. This was typical of higher growth temperatures, where the shell thickness was extremely nonuniform, completely diminishing at the bottom third of the NWs, at a temperature of 450 °C. The shell was grown at a slow rate, relating to a bulk epitaxial growth rate of 0.15 μm/h to ensure high quality epitaxial growth. Furthermore, we found that coating of core wires longer than 5 μm resulted in significant bending and warping during the shell growth. Therefore, we kept the length of the core InAs NWs no larger than 6 μm by limiting the net time of the core growth to 1 h. We studied NWs from eight different samples having a core diameter of at least a couple of tens of nanometers varying mostly the shell growth time (noting that a variation in the core diameter is anyhow obtained due to the distribution in the diameter of the gold droplets).

The morphological characteristics of the NWs were studied by scanning electron microscopy (SEM) (Zeiss Supra 55 at 2 kV). Images of three different views were taken: at 45°, in cross-section, and a top view. The structural properties were analyzed by transmission electron

Received: March 28, 2011
Revised: July 17, 2011
Published: August 01, 2011

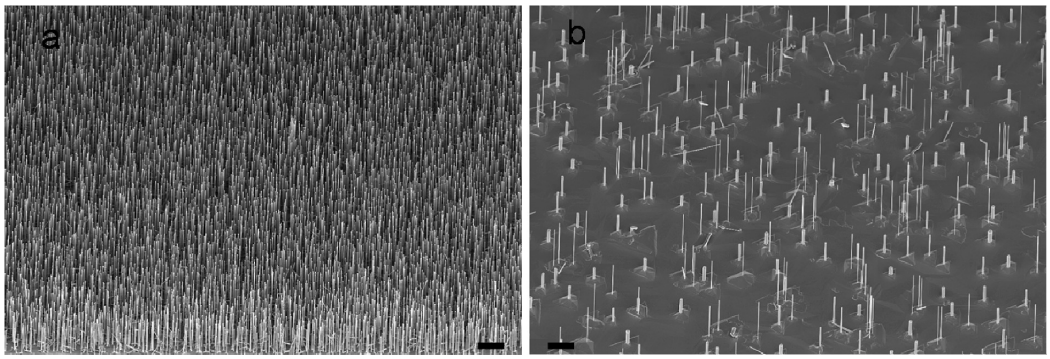

Figure 1. SEM images of as-grown InAs NWs grown on (111)B InAs at two substantially different densities. The evaporated gold layer was annealed at 550 °C (a) and 600 °C (b), respectively. Scale bar is 2 μm.

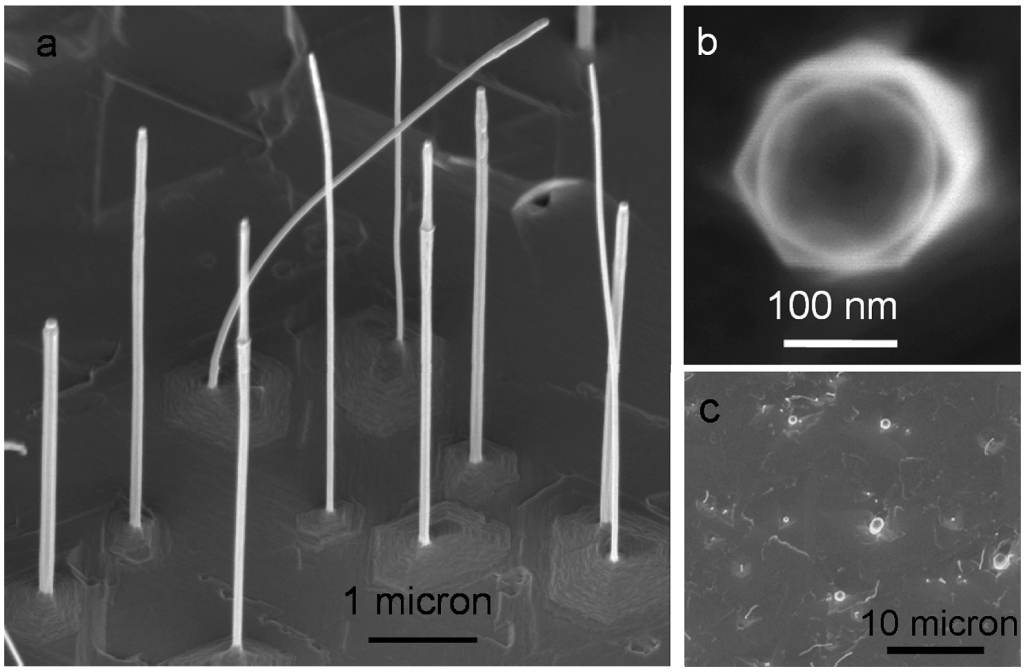

Figure 2. (a) SEM image of as-grown InAs/GaAs core−shell NWs taken at 45 deg. (b) Top view of a single, thick NW (where imaging is not smeared by vibrations). The shell facets are parallel to the (011) cleavage plane of the InAs substrate. (c) Top view SEM image of the as-grown sample of InAs/GaAs core−shell NWs.

microscopy (TEM) using a Philips CM120 microscope operating at 120 kV and an FEI Tecnai F30 UT high resolution transmission electron microscope (HRTEM) operating at 300 kV. Scanning transmission electron microscopy (STEM) (FEI Tecnai F20 at 200 kV) using high angle annular dark field detector (HAADF) in conjunction with energy dispersive spectrometry (EDS) (EDAX) were used for elemental analysis. Samples of as-grown NWs were prepared by dispersing the NWs in ethanol, using an ultrasonic bath for 1 min, followed by placing a 5 μL drop onto a 300 mesh carbon/collodion/Cu or lacy carbon/Cu grid.

Cross-section samples for TEM were prepared using a Helios NanoLab600 focused ion beam (FIB) microscope from FEI. A bundle of NWs were collected by an Omniprobe micromanipulator and embedded in C and Pt. A coarse cross-section lamella was cut from the center of the NW bundle and transferred to a TEM grid. The lamella was then thinned down in steps with a focused ion beam (FIB) voltage of 30, 5, and 2 kV to a final thickness of less than 50 nm.

RESULTS AND DISCUSSION

Au-assisted growth of bare InAs NWs has been reported before by a few groups.[18−21] The first requirement for coating of NWs is to ensure that the core wires are grown at reasonably low density in order to avoid shadowing during the shell growth. This is normally done either using photolithography or by spreading of gold nano particles. Nevertheless, a low NWs density can be achieved by careful adjustment of the thickness of the gold layer evaporated on the InAs substrate and more importantly the temperature at which it is heated to form the droplets (Au annealing temperatures used were 600 and 550 °C for the low and high density of nanowires, respectively). It seems that Oswald ripening takes place during the formation of the gold droplets, which is enhanced at higher temperature and is responsible for the diluted density of NWs. During this process, particularly large droplets are formed having a slow growth rate, as well as small ones that grow faster and provide the diluted

population of long NWs. SEM images of InAs NWs grown on (111)B InAs at a high density and at a significantly lower density can be seen in Figure 1, panels a and b, respectively. The 4−5 μm long and 30−60 nm thick InAs NWs thus grown have a wurtzite structure with occasional stacking faults concentrated mostly at the top 30% of the NWs length. The InAs NWs cross-section is often hexagonal as seen from top view SEM images with typical $\{1\bar{1}00\}$ side facets, confirmed by a 30 deg rotation relative to the (110) cleavage plane of the substrate (which means that NWs spread on the TEM grid should be tilted by 30 deg in order to obtain alignment suitable for observing the stacking faults). Occasionally, the SEM top view exposes either a more highly faceted (12 facets) or round shape. It is worth mentioning here that GaAs NWs grown by the same method typically have a prominent $\{11\bar{2}0\}$ set of facets (requiring no tilting for observation of the stacking faults). We will see later that indeed the growth of the GaAs shell follows this behavior with respect to the underlying core NW.

The low density InAs NWs were coated with a GaAs layer, producing a shell of 5−30 nm, respectively. The coating temperature was adjusted to ensure a uniform coating along the NW. Indeed, we see that after coating the wires maintain a rod shape with negligible tapering. This can be seen in Figure 2a, which is an SEM image taken at 45 deg to the surface and more clearly in low magnification TEM imaging (shown later, in Figure 4a). The top view SEM image (Figure 2b) hints at the possibility that there is a 30 deg facet rotation during the growth of the shell from $\{1\bar{1}00\}$ to $\{11\bar{2}0\}$ side facets. Substantiated by additional results, this is further discussed at the end of this manuscript. The initial signs of the strain resulting from the large mismatch between InAs and GaAs assuming the wurtzite structure (growing in the [0001] direction) can be seen in the form of some warping of the NWs, which occurs more severely in thin wires than in thick ones and in long wires as compared to short ones (Figure 2a).

Next we confirm the existence of a core−shell structure by STEM imaging using an HAADF detector as well as by an EDS line scan as shown in Figure 3. The brightness difference between the core and the shell in the STEM−HAADF images is hardly distinguished since the gold tip determines the contrast due to its high atomic number. Two EDS line profiles of As, In, and Ga were recorded across the NW and along its tip and are displayed below the STEM image. The profile measured across the NW clearly shows a uniform As distribution, while In is peaking at the center of the wire and Ga peaks symmetrically on both sides of the core. The profile taken along the tip shows a decrease in the In concentration to zero and a residual uniform concentration within the gold. The Ga concentration increases simultaneously with the decrease in the In and is mostly absent in the gold tip. The arsenic line is constant declining at the interface between the NW and the gold and is mostly absent within the gold, except on its skin where there seems to be residual As depicted by the small As peak on gold circumference. Thus, along with the termination of the growth of the InAs core, some axial growth of pure GaAs takes place, which continues during the coating process.[22,23] The section of pure GaAs at the top of the wire is also manifested by the 1:1 ratio of As to Ga after the In concentration reduces to zero. GaAs growth at the tip extended between 100 and 500 nm depending on the shell growth time as can be seen in the TEM images as well as the EDS scan (Figure 3).

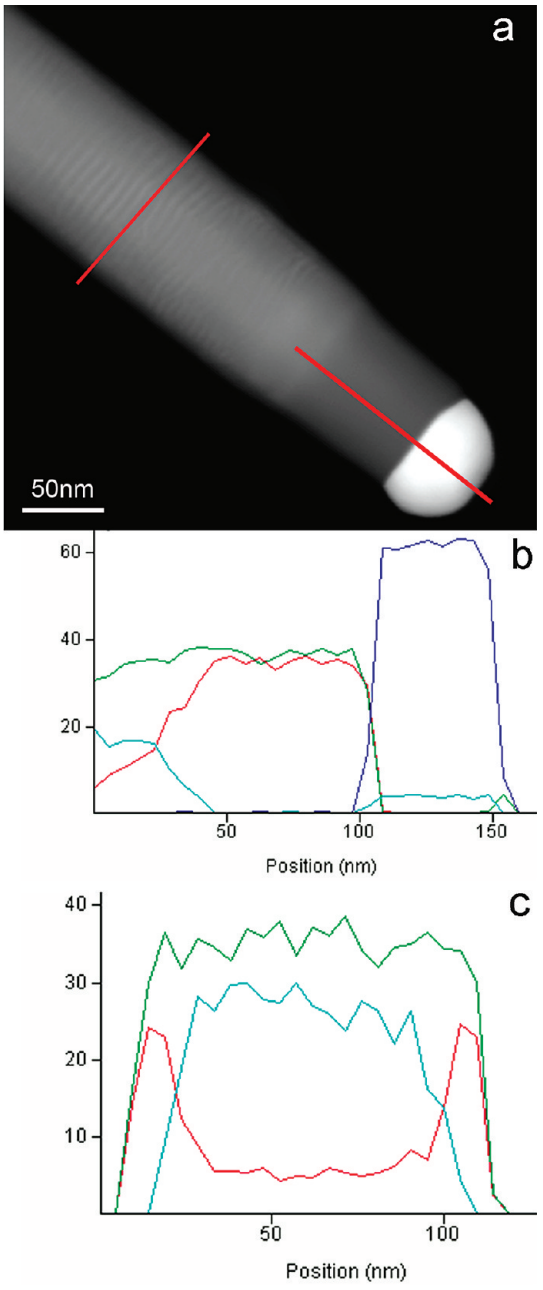

Figure 3. (a) STEM−HAADF image taken from the top part of an InAs/GaAs core−shell NW and the corresponding EDS line scans, measured (b) along its tip and (c) across the NW (as indicated by the red lines, respectively). Element intensity profiles relate to As (green), Ga (red), In (light blue), and Au (blue). The fine structure seen vaguely on the NW may result from some interference in the overlapping region of the two lattices.

This is supported by the termination of the Moiré fringe pattern at the top of the core−shell NWs, which is indicative of the interface between the InAs core and the GaAs growing at the tip.

An as-grown core−shell wire can be seen in Figure 4a, depicting a uniform diameter along the 5 μm long coated NW and a smooth and uniform surface along its sides, in comparison with some previously published results where InAs/GaAs core−shell NWs have been grown with significant tapering and/or irregular side walls.[15]

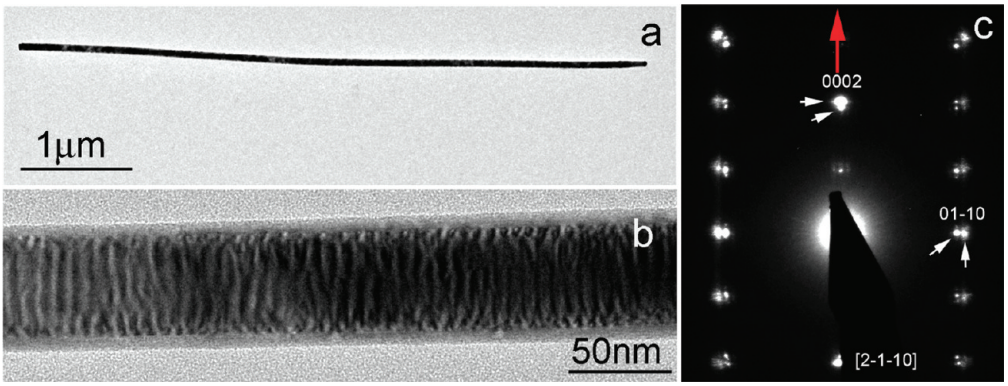

Figure 4. InAs/GaAs core−shell NW. (a) TEM at low magnification showing the whole rod shape NW. (b) TEM from the center of the NW showing the typical Moiré pattern. (c) Electron diffraction taken from the center of the NW. The small arrows point to the split diffraction spots, and the large red arrow indicates the respective growth direction.

Scheme 1. A Schematic Illustration of the Two Types of Edge Dislocations Line (left) and Loop (right), Expected to Be Present in a Core/Shell NW of Two Highly Mismatched Materials[a]

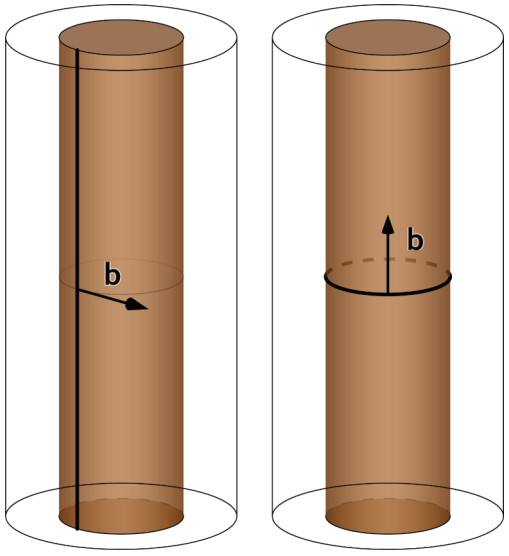

[a] Reprinted with permission from ref 27 (DOI: 10.1088/0268-1242/25/2/024006). Copyright 2010 Institute of Physics.

Low magnification TEM images of the InAs/GaAs core−shell NWs show a typical Moiré pattern, which results from interference of the two relaxed crystal lattices (Figure 4b). The semiperiodic Moiré pattern along the NW axis is confined to the core region where the two crystal lattices of InAs and GaAs overlap, while the apparently relaxed shell is clear of any interference features. We can relate the spacing of the Moiré fringes (D) to the corresponding d-spacing of the two overlapping crystal lattices (d), where $D = d_1{}^*d_2/(d_1 - d_2)$[24] ($d_1$ and d_2 relate to the lattice spacing of InAs and GaAs in our case). More explicitly we used the experimental D and d_1 of InAs (measured by X-rays on InAs whiskers[25]) to calculate a new d_2 value of the partially relaxed lattice of GaAs (relative to the lattice constant of wurtzite GaAs taken from the Inorganic Crystal Structure Database), assuming only d_2 of the GaAs shell changes. The misfit δ between the two lattices was then derived using the relation $\delta = (d_1 - d_2)/d_1$. The observed Moiré fringe periodicity is 7−8.5 nm which corresponds to a lattice misfit of 4.5 ± 0.5%. This value is significantly lower than the theoretical mismatch of 8% obtained when calculated, using the 0002 reflections of the wurzite structures of InAs (0.351 nm)[25] and GaAs (0.322 nm).[26] The existence of two adjacent relaxed lattices is further manifested by the splitting of the spots in the electron diffraction pattern (Figure 4c), proving the crystal structure of the core and the shell to be wurtzite, in agreement with previously published work by Paladugu et al.[15] Interestingly, two different misfit values were obtained when measuring the splitting of the spots in the diffraction pattern taken along the $[2\bar{1}\bar{1}0]$ zone axis: 4 ± 0.5% when using the 0002 reflections and 6.2 ± 1.0% when using the $01\bar{1}0$ type reflections, indicating that the misfit along the NW is smaller than around its circumference [the misfit values from the diffraction data where deduced by measuring the experimental d_1 and d_2 (from two adjacent diffraction spots of InAs and GaAs, respectively) and inserting them into the formula $\delta = (d_1 - d_2)/d_1$. This observation suggests that only partial lattice relaxation occurs along the NW axis and more complete relaxation takes place around it. Since the core diameter of the NWs we studied was significantly larger than the predicted critical diameter for dislocations formation we did not observe any fully strained wires.[27−29]

Theoretical calculations on strained core−shell NWs show that the strain is expected to be relieved by forming two sets of edge dislocations as illustrated in Scheme 1.[27,28] Namely, one set of line edge dislocations is expected to form along the wire and the other set of loop edge dislocations is expected to form within the shell along the NW perimeter. The line and loop dislocations will relax the strain in the radial and axial directions, respectively.

HRTEM imaging of NWs clearly shows a semiperiodic set of edge dislocations emerging from the interface between the core and the shell on either side of the core, perpendicular to the growth direction and all along the shell width. At high magnification (>500 k), it is possible to observe the general location where the extra plane originates. This is the projection of the edge dislocation loops lying within the shell, surrounding the core at a periodicity that relates to the misfit between the lattice of the core and that of the shell along the ⟨0001⟩ direction. This is in contrast to the theoretical prediction that in the case of the wurzite structure, only the line dislocations are expected to be seen.[29] The loop edge dislocations that we see when viewed from the side facets are spaced on average about 7−8 nm from each other,

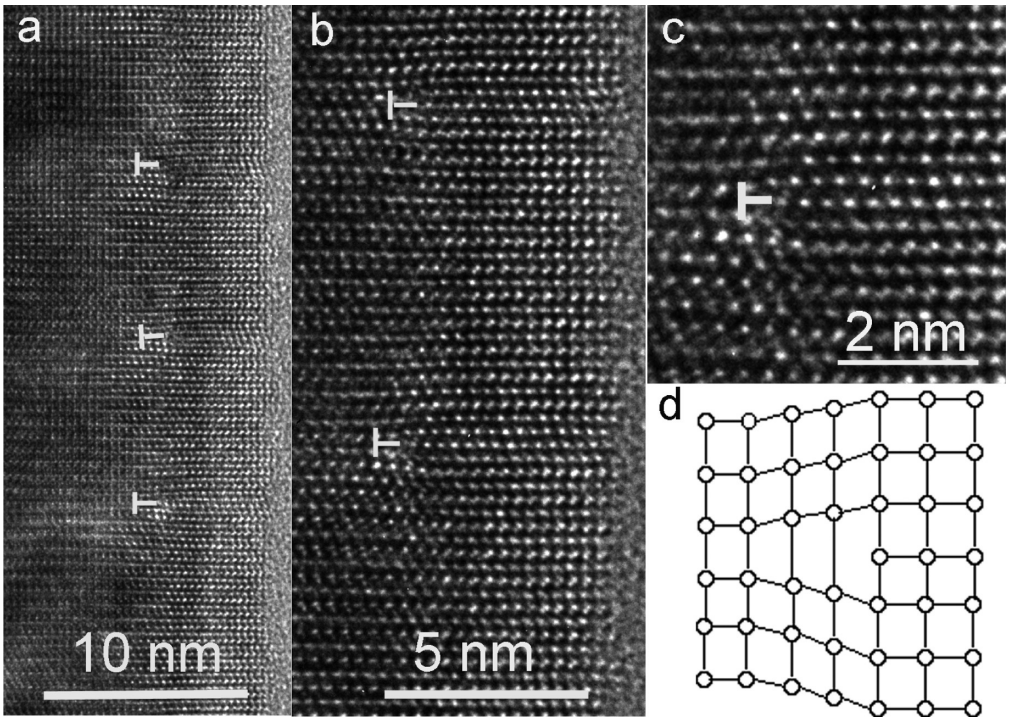

Figure 5. (a) HRTEM image of the core−shell interface region of InAs/GaAs NW, showing three edge dislocations. . (b) Higher magnification of two of the dislocations shown in (a). (c) A single dislocation revealing the extra lattice plane in the shell region (dislocations are marked by T). Note that the dislocations Burger's vector points in the ⟨0001⟩ direction. (d) A schematic drawing of an edge dislocation.[30]

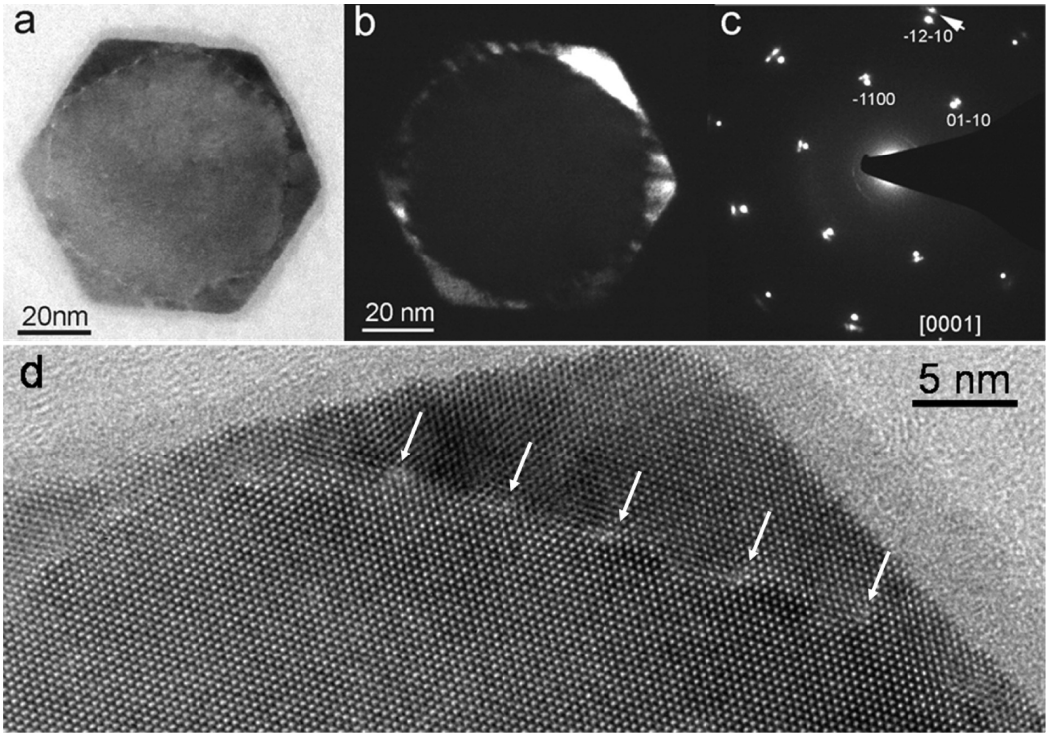

Figure 6. TEM of a cross-section of an InAs/GaAs core−shell NW: (a) bright field image, (b) dark field image obtained using the $\bar{1}2\bar{1}0$ GaAs diffraction (indicated by the arrow), (c) electron diffraction from the [0001] zone axis, (d) high magnification of one corner showing the facets build up and the dislocations formation along the interface (seen as bright periodic spots). White arrows point at the dislocation nodes.

which means that every 20−25 lattice planes (0002) there is an extra plane. This number extracted from the HRTEM images fits roughly to the semiperiodicity of the Moiré fringes ($D = 7-8.5$ nm), both suggesting a lower misfit value ($4.5 \pm 0.5\%$) than expected.

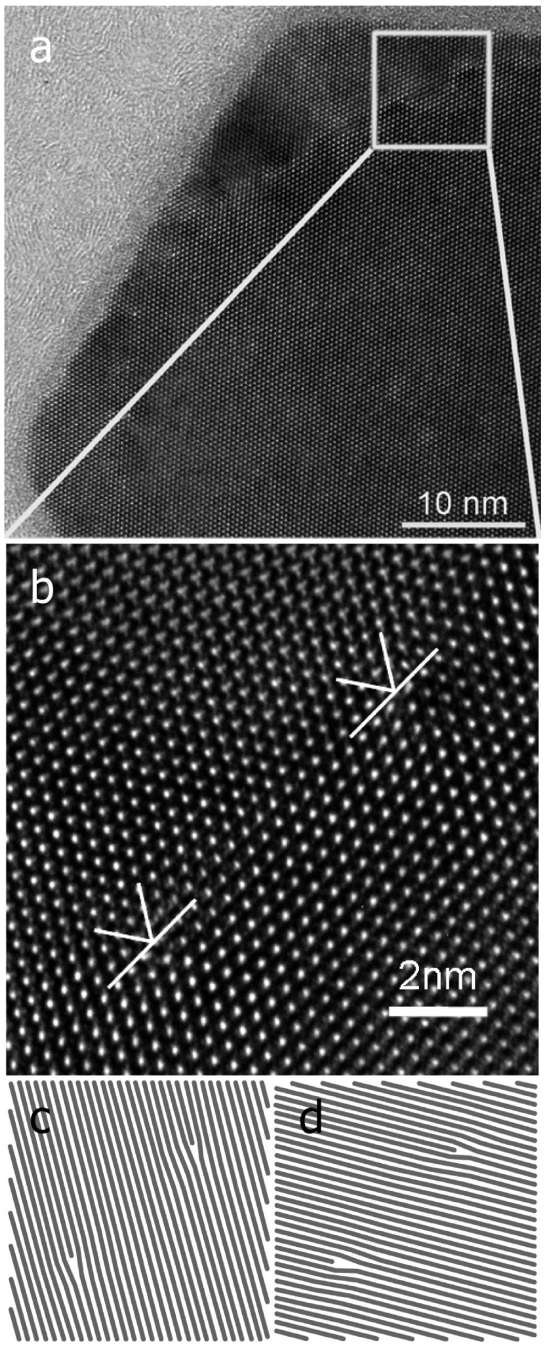

Figure 7. (a) HRTEM image of a cross-section of an InAs/GaAs core−shell NW at the interface region between the shell and the core. (b) Higher magnification of the region in the square box in (a), revealing two paired dislocations (marked by V) with Burger's vectors pointing in the <11$\bar{2}$0> and <2$\bar{1}\bar{1}$0> directions. Panels (c) and (d) are schematic illustrations of the lattice planes depicting the extra ones.

Figure 5a shows clearly three such dislocations at high magnification, where the emerging point of the dislocations is marked with a white T. Two of the dislocations are further magnified in Figure 5b. Figure 5c shows a HRTEM image of a single dislocation described schematically in (d). Interestingly, careful inspection of the HRTEM images reveals that in many dislocations the extra nucleated planes tend to stack in a zinc blende type stacking. This tendency can be rationalized by the differences between the mismatch values along the [111] axis in zinc blende (6.6%) and that of wurtzite, along the corresponding [0001] axis (8%).[25,26] Namely, the extra nucleated plane can be more easily accommodated in a zinc blende type stacking.

In order to trace the line edge dislocations, it was necessary to produce cross-sections taken from the center of the core−shell NWs and thinned to a thickness (<50 nm) that allows high resolution TEM imaging. The first thing that is apparent from the bright and dark field TEM images (dark field image taken using the $\bar{1}2\bar{1}0$ GaAs diffraction (Figure 6a,b)) is the faceting of the exterior of the NWs, as well as the strain induced Moiré pattern. A closer look at one of the cross-section corners reveals a well-defined build up of the two adjacent facets and a set of dislocation nodes situated along the interface (Figure 6d pointed with white arrows). Electron diffraction (Figure 6c) taken from the [0001] zone axis shows a typical hexagonal pattern as expected for the wurtzite structure when observed from this direction. Splitting of the diffraction spots was also observed, corresponding to a misfit value of 6.5 ± 0.5%. Figure 7a shows an HRTEM image taken from a cross-section of an InAs/GaAs core−shell NW at the interface region between the shell and the core. When imaging the cross-section under higher magnification (>500 k), it is possible to spot clearly a couple of line edge dislocations, emerging at the interface between the core and the shell proceeding toward the NW edge (Figure 7b, marked with a white V). A closer look exposes the fact that the line misfit dislocations are paired with two inclined misfit planes emerging from the node and lying at 60° to each other. Such paired misfit dislocations are well-known to have formed at planar highly mismatched interfaces[31,32] but to the best of our knowledge have not been shown before in a cylindrical system. The distance between these dislocations is 15−17 lattice planes that correspond to a misfit of about 6.2%, in agreement with the values obtained from the electron diffraction patterns. We did not see an effect of the core diameter either on the loop or on the line dislocations, in the range of core diameters that we have checked which ranged between 30 and 80 nm. It is noteworthy that according to theoretical work such an effect is expected when the core diameter is smaller than 10 nm.[27−29]

The radial (6 ± 1%) and axial (4 ± 0.5%) misfits indicate a nonuniform lattice relaxation. Both values clearly differ from the mismatch of 8% calculated using the InAs and GaAs parameters taken from refs 25 and 26, respectively. Nevertheless, it is important to emphasize that different experimental lattice parameters were measured for wurtzite GaAs formed by pressurizing zinc blende bulk material.[33] Even though these experimental parameters are not necessarily applicable to NWs, they suggest a mismatch of only 6.6%, which implies a full radial strain relaxation and a partial axial strain relief.

STEM−HAADF imaging of the cross-section as well as the respective EDS analysis verified the elemental composition along the diameter, as can be seen in Figure 8. The distribution of In, Ga, and As along the diameter can be clearly seen, where the As is quite constant, the In is concentrated at the center of the NW and the Ga peaks on both sides of the core.

Finally, we relate to the respective orientation between the core and the prominently faceted shell since we sometimes see evidence for a relative rotation of the facets by 30°. This is obvious from the overview bright field TEM image of the cross-section seen in Figure 6a and more clearly from the enlarged image in Figure 6d depicting the build-up of two new facets over the original facet of the core. Note that a hint for this rotation can be seen in the top view SEM image of these NWs seen in

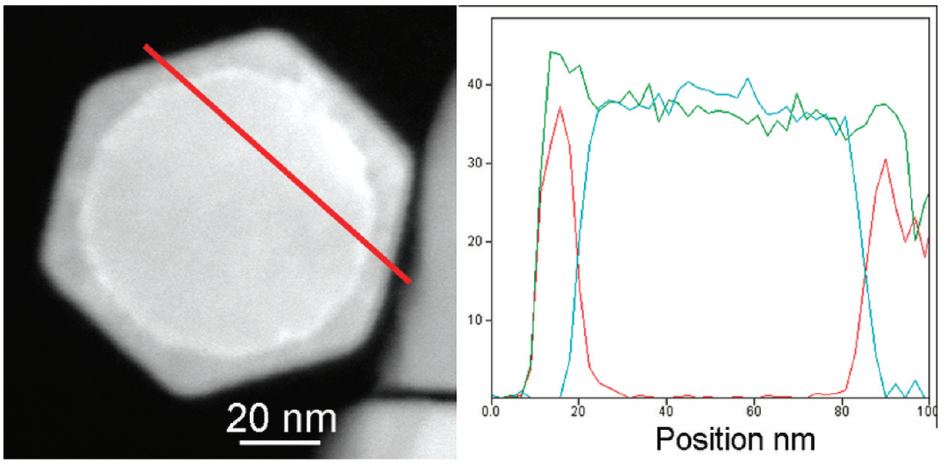

Figure 8. STEM−HAADF image of a cross-section of an InAs/GaAs core−shell NW and the corresponding EDS line scan measured along the diameter of the NW (marked by red line). Element intensity profiles: As (green), Ga (red), In (light blue).

Figure 2b as a smeared triangular shadow extending from a couple of the facets. We often note that the shape of the core which appears in the NW cross-section is not necessarily hexagonal but either composed of 12 facets or completely rounded (as seen in numerous samples produced from bare InAs NWs). Namely, some of the InAs NWs lack the prominent faceting typical of NWs having the wurtzite structure but instead have a cylindrical shape where the facets did not develop either because of the growth conditions or because the NW diameter is too small for the facets to develop. Since the shell forms in a two-dimensional growth process,[34] it is also possible to assume that there could be some smearing of the interface between the core and the shell, during the shell growth, in a process that resembles a migration enhanced epitaxy. Such migration enhanced epitaxy has indeed been shown to replace group III atoms in slowly growing two-dimensional surfaces.[35]

CONCLUSIONS

In summary, we demonstrated the growth of uniform, rod shape InAs/GaAs core−shell heterostructure NWs by the Au-assisted VLS-MBE, in spite of the large mismatch. Such NWs are good candidates for electronic and optical devices where carriers are confined to the InAs core and the surface is in situ passivated with a wide band gap material. The core−shell NWs are partially relaxed, forming paired line dislocations and loop edge dislocations within the shell, along the NW, and around it, respectively. The radial ($6 \pm 1\%$) and axial ($4 \pm 0.5\%$) misfits indicate a nonuniform relaxation process and were found to be different from the nominal mismatch. Thus, the strain relaxation is partial and is larger in the radial as compared to the axial direction. We relate some discrepancy between this work and previously published results[15,16] to the high quality of our InAs/GaAs core shell nanowires. Namely, the highly uniform and smooth surface-coating, the lack of significant warping or bending, and a very low density of stacking faults.

AUTHOR INFORMATION

Corresponding Author

*Phone: 972-8-9342585; fax: 972-8-9344128; e-mail: hadas.shtrikman@weizmann.ac.il.

ACKNOWLEDGMENT

The authors are thankful to Moty Heiblum, head of the Braun Center for Submicron Research, for making the NWs project possible. We are grateful to Perla Kacman from the Institute of Physics at the Polish Academy of Sciences and to Ernesto Joselevich for fruitful and stimulating discussions and critical reading of this manuscript. Nissim Ofek's contribution to the understanding of some of the results is invaluable. We are grateful to Michael Fourmansky for professional support in the NWs MBE lab. The work was partly supported by the Israeli Science Foundation Grant No. 530/08 and the Israeli Ministry of Science Grant No. 3-66799. The transmission electron microscopy studies were conducted at the Irving and Cherna Moskowitz Center for Nano and Bio-Nano Imaging at the Weizmann Institute of Science.

REFERENCES

(1) Jespersen, T. S.; Aagesen, M.; Sorensen, C.; Lindelof, P. E.; Nygard, J. *Phys. Rev. B* **2006**, *74*, 233304.
(2) Csonka, S.; Hofstetter, L.; Freitag, F.; Oberholzer, S.; Schoenenberger, C.; Jespersen, T. S.; Aagesen, M.; Nygard, J. *Nano Lett.* **2008**, *8*, 3932–3935.
(3) Fasth, C.; Fuhrer, A.; Samuelson, L.; Golovach, V. N.; Loss, D. *Phys. Rev. Lett.* **2007**, *98*, 266801.
(4) Lutchyn, R. M.; Sau, J. D.; Das Sarma, S. *Phys. Rev. Lett.* **2010**, *105*, 077001.
(5) Oreg, Y.; Refael, G.; von Oppen, F. *Phys. Rev. Lett.* **2010**, *105*, 177002.
(6) Lauhon, L.; Gudiksen, M.; Wang, C.; Lieber, C. *Nature* **2002**, *420*, 57–61.
(7) Jiang, X.; Xiong, Q.; Nam, S.; Qian, F.; Li, Y.; Lieber, C. M. *Nano Lett.* **2007**, *7*, 3214–3218.
(8) van Tilburg, J. W. W.; Algra, R. E.; Immink, W. G. G.; Verheijen, M.; Bakkers, E. P. A. M.; Kouwenhoven, L. P. *Semicond. Sci. Technol.* **2010**, *25*, 024011.
(9) Mohan, P.; Motohisa, J.; Fukui, T. *Appl. Phys. Lett.* **2006**, *88*, 013110.
(10) Niquet, Y. M. *Nano Lett.* **2007**, *7*, 1105–1109.
(11) Niquet, Y. M. *Physica E* **2007**, *37*, 204–207.
(12) Paladugu, M.; Zou, J.; Guo, Y.-N.; Zhang, X.; Joyce, H. J.; Gao, Q.; Tan, H. H.; Jagadish, C.; Kim, Y. *Angew. Chem., Int. Ed.* **2009**, *48*, 780–783.
(13) Paladugu, M.; Zou, J.; Guo, Y.-N.; Zhang, X.; Kim, Y.; Joyce, H. J.; Gao, Q.; Tan, H. H.; Jagadish, C. *Appl. Phys. Lett.* **2008**, *93*, 101911.
(14) Paladugu, M.; Zou, J.; Guo, Y.-N.; Zhang, X.; Joyce, H. J.; Gao, Q.; Tan, H. H.; Jagadish, C.; Kim, Y. *Appl. Phys. Lett.* **2008**, *93*, 201908.

(15) Paladugu, M.; Zou, J.; Guo, Y. N.; Zhang, X.; Joyce, H. J.; Gao, Q.; Tan, H. H.; Jagadish, C.; Kim, Y. *Nanoscale Res. Lett.* **2009**, *4*, 846–849.
(16) Kavanagh, K. L.; Salfi, J.; Savelyev, I.; Blumin, M.; Ruda, H. E. *Appl. Phys. Lett.* **2011**, *98*, 152103.
(17) Shtrikman, H.; Popovitz-Biro, R.; Kretinin, A. V.; Kacman, P. *IEEE J. Sel. Top. Quantum Electron.* **2010**, DOI: 10.1109/JSTQE.2010.2053920.
(18) Caroff, P.; Dick, K. A.; Johansson, J.; Messing, M. E.; Deppert, K.; Samuelson, L. *Nat. Nanotechnol.* **2009**, *4*, 50–55.
(19) Tchernycheva, M.; Travers, L.; Patriarche, G.; Glas, F.; Harmand, J.-C.; Cirlin, G. E.; Dubrovskii, V. G. *J. Appl. Phys.* **2007**, *102*, 094313.
(20) Dayeh, S. A.; Susac, D. A.; Kavanagh, K. L.; Yu, E. T.; Wang, D. *Adv. Funct. Mater.* **2009**, *19*, 2102–2108.
(21) Dick, K. A.; Thelander, C.; Samuelson, L.; Caroff, P. *Nano Lett.* **2010**, *10*, 3494–3499.
(22) Ohlsson, B.; Bjork, M.; Persson, A.; Thelander, C.; Wallenberg, L.; Magnusson, M.; Deppert, K.; Samuelson, L. *Physica E* **2002**, *13*, 1126–1130.
(23) Hiruma, K.; Murakoshi, H.; Yazawa, M.; Katsuyama, T. *J. Cryst. Growth* **1996**, *163*, 226–231.
(24) Fultz, B.; Howe, J. M. *Transmission Electron Microscopy and Diffractometry of Materials*; Springer-Verlag: New York, 2002.
(25) Takahash, K; Moriizum, K. *Jpn. J. Appl. Phys.* **1966**, *5*, 657.
(26) Yeh, C.-Y.; Lu, Z. W.; Froyen, S.; Zunger, A. *Phys. Rev. B* **1992**, *46*, 10086–10097.
(27) Kavanagh, K. L. *Semicond. Sci. Technol.* **2010**, *25*, 024006.
(28) Raychaudhuri, S.; Yu, E. T. *J. Vac. Sci. Technol. B* **2006**, *24*, 2053–2059.
(29) Raychaudhuri, S.; Yu, E. *J. Appl. Phys.* **2006**, *99*, 114308.
(30) *MAST Modules*; Department of Materials Science and Engineering, University of Illinois: Urbana-Champaign, IL; http://matse1.matse.illinois.edu/metals/prin.html.
(31) Kawai, T.; Yonezu, H.; Saito, D.; Yokozeki, M.; Pak, K. *Jpn. J. Appl. Phys.* **1994**, *33*, L1740–L1743.
(32) Shiramine, K.; Horisaki, Y.; Suzuki, D.; Itoh, S.; Ebiko, Y.; Muto, S.; Nakata, Y.; Yokoyama, N. *J. Cryst. Growth* **1999**, *205*, 461–466.
(33) McMahon, M. I.; Nelmes, R. J. *Phys. Rev. Lett.* **2005**, *95*, 215505.
(34) Cornet, D. M.; LaPierre, R. R. *Nanotechnology* **2007**, *18*, 385305.
(35) Yamaguchi, H.; Horikoshi, Y. *J. Appl. Phys.* **1990**, *68*, 1610–1615.